ARTICLE NO. 79-4103

Interaction between the Unsteady Boundary Layer and Inviscid Hot Flow in a Shock Tube

D. Zeitoun* and M. Imbert†
University of Provence, St. Jerome Center, Marseille, France

A numerical calculation is presented for the flow in a low-pressure shock tube. The evolution of the hot flow quantities due to mutual interaction between the boundary layer and inviscid hot flow are taken into account. A better knowledge of the unsteady evolution of this hot flow is so obtained, including the distribution of all parameters at the limiting regime. The computational results, with Argon as a driven gas, are in agreement with the different experimental results at usual measurement stations.

Nomenclature

a = sound velocity
D = shock tube diameter
H = enthalpy
L = separation distance between shock and contact surface
Lm = maximum separation distance
$m(x,t)$ = mass loss term
M_s = shock Mach number
P = pressure
Pr = Prandtl number
R = shock tube radius
$\hat{R}$ = perfect gas constant
S = entropy
T = temperature
u = axial flow velocity
U = flow velocity
U_s = shock velocity
$\bar{U}$ = $U_s - U$ = flow velocity in a shock-fixed coordinate system
v = radial flow velocity
(x,y,t), (x,r,t) = laboratory coordinate system
W = density ratio across the shock
γ = ratio of specific heats
δ = boundary-layer thickness
$\delta^* = \int_0^\delta \left(1 - \frac{\rho u}{\rho_e U_e}\right)\left(1 - \frac{y}{R}\right) dy$ = displacement thickness
$\delta_\rho^* = \int_0^\delta \left(1 - \frac{\rho}{\rho_e}\right)\left(1 - \frac{y}{R}\right) dy$ = density displacement thickness
ρ = density
μ = viscosity
τ_R = test time
τ_m = maximum test time
τ_{TH} = test time in ideal shock tube theory

Subscripts

c = conditions at the contact surface
e = conditions in the inviscid hot flow
i = conditions from ideal shock tube theory
ℓ = conditions at the limiting regime
S = conditions immediately behind the shock wave
W = conditions at the wall
1 = conditions in the undisturbed flow ahead of the shock

Received Aug. 14, 1978; revision received Feb. 20, 1979.

Index categories: Nonsteady Aerodynamics; Jets, Wakes, and Viscid-Inviscid Flow Interactions.

*Research Engineering, Dept. of Mathematics, Fluid Dynamics and Thermophysics Lab.

†Assistant, Dept. of Mathematics, Fluid Dynamics and Thermophysics Lab.

I. Introduction

THE interaction between the inviscid flow and the wall boundary layer in a shock tube is characterized by an attenuation of the shock wave, an acceleration of the contact surface, a nonuniform flow, and a separation distance approaching a limiting value when the shock and the contact surface move at the same velocity. Duff[1] was apparently the first to observe this phenomenon and explained it in terms of leakage of hot shocked gas through the boundary layer past the interface. Roshko[2] obtained analytical estimates for the separation distance. Hooker[3] improved Roshko's results. In these studies, the interaction may be defined in terms of a parameter β proportional to the boundary-layer thickness. The observed discrepancy between theory and experiments may be explained by the approximate nature of the solution of the boundary-layer equations used to calculate this parameter (the external freestream is assumed constant, the shock wave moves with constant velocity).

Mirels[4,5] improved the values of the parameter β. He took account of the mutual interaction between the boundary layer and the freestream, but the flow between the shock and the contact surface remained steady in the shock-fixed coordinate system. Ackroyd,[6] in a study of shock tube test time, applied momentum integral boundary-layer solutions presented by Bernstein[7] and included the variation of the contact surface velocity.

Musgrove et al.[8] developed a constant shock speed analysis and a linearized unsteady analysis to obtain asymptotic solutions which predict finite limiting test times. Mirels[9] reviewed the main features of the boundary-layer induced, shock tube flow nonuniformity. However, none of these theories can properly predict the unsteady variations of the freestream and boundary layer, since they do not take account of all modifications induced by mutual interaction.

From Spence and Wood's[10] analysis of the determination of the mass loss term, Sides and Brun[11] presented numerical results for the unsteady freestream, but the boundary-layer displacement thickness was calculated from the steady boundary-layer equations without pressure gradient. Brun and Imbert[12] improved these results, they integrated the boundary-layer equations with a local similarity method.

In the present paper, the unsteady evolution of viscous inviscid hot flow up to the asymptotic regime is investigated by taking account of the spatio-temporal variations of the freestream and the boundary layer. The one-dimensional unsteady equations of the freestream are computed by the method of characteristics (Hartree's method) and the axisymmetric unsteady laminar boundary-layer equations are computed by a second-order finite-difference scheme. Both equation systems are coupled with the mass loss term which appears in the continuity equation. The application of these numerical methods to argon as a test gas enables us to determine the unsteady evolution of the freestream and boundary-layer parameters and to find an expression of limiting values of hot flow length and test time which are compared to available experimental results.

II. Flow Equations

A. Freestream Equations

It has been shown that the equations of the freestream in a tube of uniform circular cross section are those of one-dimensional unsteady flow[13] if the boundary-layer thickness is small in comparison with the diameter. The right term $m(x,t)$ of the continuity equation represents the mass loss of the freestream across the boundary layer [system I, Eqs. (1)]:

Continuity

$$\frac{\partial \rho_e}{\partial t}+\frac{\partial}{\partial x}\rho_e U_e=\frac{2}{R}\left\{\frac{\partial}{\partial t}\int_0^{\delta}(\rho_e-\rho)\left(1-\frac{y}{R}\right)\mathrm{d}y+\frac{\partial}{\partial x}\int_0^{\delta}(\rho_e U_e-\rho u)\left(1-\frac{y}{R}\right)\mathrm{d}y\right\}=m(x,t) \tag{1a}$$

Momentum

$$\rho_e\left(\frac{\partial U_e}{\partial t}+U_e\frac{\partial U_e}{\partial x}\right)+\frac{\partial P_e}{\partial x}=0 \tag{1b}$$

Energy

$$\frac{\partial S}{\partial t}+U_e\frac{\partial S}{\partial x}=0 \tag{1c}$$

State

$$P_e=\rho_e\hat{R}T_e \tag{1d}$$

where δ is the boundary-layer thickness, and e refers to inviscid edge values. The equations are coupled with the boundary-layer equations in order to determine the quantity $m(x,t)$.

B. Boundary-Layer Equations

The laminar axisymmetric unsteady boundary-layer equations in a laboratory cylindrical coordinate system [system II, Eqs. (2)] are

Continuity

$$\frac{\partial \rho r}{\partial t}+\frac{\partial \rho u r}{\partial x}+\frac{\partial \rho v r}{\partial r}=0 \tag{2a}$$

Momentum

$$\rho\left(\frac{\partial u}{\partial t}+u\frac{\partial u}{\partial x}+v\frac{\partial u}{\partial r}\right)=-\frac{\partial P}{\partial x}+\frac{1}{r}\frac{\partial}{\partial r}\left(\mu r\frac{\partial u}{\partial r}\right)\quad\text{and}\quad\frac{\partial P}{\partial r}=0 \tag{2b}$$

Energy

$$\rho\left(\frac{\partial H}{\partial t}+u\frac{\partial H}{\partial x}+v\frac{\partial H}{\partial r}\right)=\frac{\partial P}{\partial t}+\frac{1}{r}\frac{\partial}{\partial r}\left\{\frac{\mu r}{P_r}\frac{\partial H}{\partial r}+\left(1-\frac{1}{P_r}\right)\mu r u\frac{\partial u}{\partial r}\right\} \tag{2c}$$

with $r=D/2-y$, $P=\rho\hat{R}T$, $\mu=\mu(T)$, the boundary conditions are: at the wall, $u=v=0$ and $H=Hw$, and at the edge, $u=U_e(x,t)$ and $H=H_e(x,t)$. Both equation systems are coupled on one side by the right terms of the continuity equation of system I and on the other side by the boundary conditions of boundary-layer equations (II).

III. Numerical Methods

A. Freestream

The constant time technique of the method of characteristics[14] is used to integrate the hyperbolic system (I) of the freestream. These equations may be written in characteristic form

$$\frac{\mathrm{d}P}{\mathrm{d}t}-\frac{2}{\gamma-1}\rho a\left(\frac{\mathrm{d}a}{\mathrm{d}t}\right)=0\ \text{on}\ \frac{\mathrm{d}x}{\mathrm{d}t}=U \tag{3a}$$

$$\frac{\mathrm{d}P}{\mathrm{d}t}+\rho a\frac{\mathrm{d}U}{\mathrm{d}t}+a^2m=0\ \text{on}\ \frac{\mathrm{d}x}{\mathrm{d}t}=U+a \tag{3b}$$

$$\frac{\mathrm{d}P}{\mathrm{d}t}-\rho a\frac{\mathrm{d}U}{\mathrm{d}t}+a^2m=0\ \text{on}\ \frac{\mathrm{d}x}{\mathrm{d}t}=U-a \tag{3c}$$

At time t the values of all variables at all grid points are known. In order to calculate them at time $t+\Delta t$, the numerical procedure requires three different meshes depending on how one calculates the shock trajectory, the position, and state of an interior point or of the ideal contact surface.

In each case, the characteristic equations are written in a finite-difference form and the coefficients in an average form. At the shock, Hugoniot relations are used, and on both sides of the interface the pressure and the velocity are assumed equal. In the driver gas flow, the boundary layer is turbulent and the displacement thickness and the corresponding mass loss term have been calculated in an approximate manner assuming for the boundary layer the form given in Ref. 15. This calculation shows that its effect on the hot flow is small in comparison with this coming from the hot flow boundary layer (see Sec. VA).

The numerical stability of the method of characteristics is obtained if Courant-Friedrich-Levy criterion is respected [$\Delta t<\min(\Delta x/a_e)$].

B. Boundary Layer

Before solving numerically the nonlinear parabolic partial differential equations of the boundary layer (II), these are transformed into a more convenient form. At first, the independent variables (x,r,t) are changed to (ξ,η,τ) defined so that

$$\xi(x,t)=\int_0^t(U_s\mathrm{d}t-x)/L(t)$$

$$\eta(x,r,t)=\frac{U_e}{\sqrt{2\theta\xi}}\int_{r-\delta}^{R}\rho r\mathrm{d}r$$

$$\tau(t)=t$$

where

$$\theta=(\rho_e U_e L(t)R^2)_s$$

$L(t)$ is the separation distance between shock and contact surface. The independent variables ξ and η are nondimensional.

Then the dependent variables u,v,H are transformed into nondimensional variables F,V,G, namely,

$$F(\xi,\eta,\tau)=u/U_e$$

$$V(\xi,\eta,\tau)=\left(\frac{\partial\xi}{\partial x}\right)^{-1}\left\{\frac{2\xi}{U_e}\frac{\partial\eta}{\partial t}+\rho v r\frac{\sqrt{2\xi}}{\sqrt{\theta}}+2\xi\frac{\partial\eta}{\partial x}F\right\}$$

$$G(\xi,\eta,\tau)=H/H_e$$

System II can now be written in the form (as system III):

$$\frac{\partial V}{\partial\eta}+2\xi\frac{\partial F}{\partial\xi}+F+K(\xi,\tau)=0 \tag{4a}$$

$$\alpha\frac{\partial F}{\partial\tau}+V\frac{\partial F}{\partial\eta}+2\xi\frac{\partial F}{\partial\xi}(F+\gamma)+\lambda\frac{\partial}{\partial\eta}\left(\Gamma\frac{\partial F}{\partial\eta}\right)+\beta_\xi\left(F^2-\frac{\rho_e}{\rho}\right)+\left(F-\frac{\rho_e}{\rho}\right)(\gamma\beta_\xi+\beta_\tau)=0 \tag{4b}$$

$$\alpha\frac{\partial G}{\partial\tau}+V\frac{\partial G}{\partial\eta}+2\xi\frac{\partial G}{\partial\xi}(F+\gamma)+\lambda\left\{\frac{\partial}{\partial\eta}\left(\frac{\Gamma}{P_r}\frac{\partial G}{\partial\eta}\right)+\frac{U_e^2}{H_e}\frac{\partial}{\partial\eta}\left(\Gamma\left(1-\frac{1}{P_r}\right)F\frac{\partial F}{\partial\eta}\right)\right\}+\beta_{H\xi}\left(F.G-\frac{\rho_e}{\rho}\right)+(\gamma\beta_{H\xi}+\beta_{H\tau})\left(G-\frac{\rho_e}{\rho}\right)=0 \tag{4c}$$

where

$$K(\xi,\tau)=-\{\gamma(\beta_\xi-1)+(\beta_\tau-\beta_{\theta\tau})\}$$

$$\gamma(\xi,\tau)=\frac{\partial\xi/\partial t}{U_e(\partial\xi/\partial x)}=-\left\{\frac{U_s}{U_e}(1-\xi)+\frac{U_{ec}}{U_e}\xi\right\}$$

$$\alpha(\xi,\tau)=\frac{2\xi}{U_e(\partial\xi/\partial x)}=-\frac{2\xi L(t)}{U_e}$$

$$\lambda(\xi,\tau)=\frac{\rho_e\mu_e U_e}{(\rho_e\mu_e U_e)_s}$$

$$\beta_\xi(\xi,\tau)=\frac{2\xi}{U_e}\frac{\partial U_e}{\partial\xi};\quad \beta_\tau=\frac{2\xi}{U_e^2(\partial\xi/\partial x)}\frac{\partial U_e}{\partial\tau}=-\frac{2\xi L}{U_e^2}\frac{\partial U_e}{\partial\tau}$$

$$\beta_{H\xi}=\frac{2\xi}{H_e}\frac{\partial H_e}{\partial\xi};\quad \beta_{H\tau}=\frac{2\xi}{U_e(\partial\xi/\partial x)H_e}\frac{\partial H_e}{\partial\tau}=\frac{2\xi L}{U_e H_e}\frac{\partial H_e}{\partial\tau}$$

$$\beta_{\theta\tau}=\frac{\xi}{U_e(\partial\xi/\partial x)\theta}\frac{\partial\theta}{\partial\tau}=-\frac{\xi L}{U_e\theta}\frac{\partial\theta}{\partial\tau}$$

$$\Gamma(\xi,\eta,\tau)=\frac{\rho\mu}{\rho_e\mu_e}\left(1-\frac{2\sqrt{2\theta\xi}}{\rho_e U_e R^2}\int_0^\infty\frac{\rho}{\rho_e}\,d\eta\right)$$

The boundary conditions are: at the wall ($\eta=0$), $F(\xi,0,\tau)=V(\xi,0,\tau)=0$, at the edge ($\eta\to\infty$), $G(\xi,\infty,\tau)=Gw$, $F(\xi,\infty,\tau)=G(\xi,\infty,\tau)=1$. At the initial time t_0, when the variables are assumed constant (the effects of the finite time of the diaphragm opening are not taken into account) and at each step $t+\Delta t$ in $\xi=0$, the set of equations is a simple reduction of system III, obtained by setting $\xi=0$ in a straightforward manner.

The integration of system III is performed in planes $\tau=$ constant starting at $\tau=\tau_0$ and in each τ plane along the line $\xi=$ constant starting at $\xi=0$ (shock wave) to $\xi=1$ (constant surface).

The discretization of equations is made at the middle point of the integrating mesh by Crank-Nicolson's finite-difference scheme. The partial derivatives are developed in such a way that the error of truncation is proportional to the square of the integration step, the nonlinear terms in the equations are linearized by the Newton-Raphson procedure.

Then the three equations are written in a finite-difference form. The numerical procedure is composed first of the resolution of the coupled continuity and momentum equations and then of the energy equation. This numerical scheme is called the Davis Coupled Scheme (D.C.S.) and Blottner[16] shows that this scheme is of second order with one iteration. The numerical procedure is described in more detail by the authors in a previous work.[17]

One of the results of this integration is the determination of the density and velocity profiles through the boundary layer necessary for the computation of the mass loss $m(\xi,\tau)$ at each ξ. From the distribution of m between the shock and the contact surface and in order to calculate this term at each x, a quadratic interpolation is used.

The application of the algorithms to the calculations of the freestream and of the boundary layer enables us to study the spatio-temporal evolution of all quantities of the hot flow. In particular, the results concerning the limiting values can be fully analyzed and may lead to a better determination of the limiting regime in a low-pressure shock tube as it will be developed hereafter.

IV. Maximum Separation Distance and Test Time

When $t\to\infty$ the flow asymptotically tends to a limiting regime for which the shock and the contact surface have the same velocity. Then in shock-fixed coordinates the hot flow is steady ($\partial/\partial t=0$), and it is possible from the freestream continuity equation, to obtain an expression for the maximum separation distance Lm and for the test time τ_m.

Thus introducing the variables (ξ,τ), the continuity equation for the inviscid flow becomes:

$$\frac{\partial}{\partial\xi}\{\rho_e(U_S-U_e)\}=\frac{2}{R}\frac{\partial}{\partial\xi}\left\{\int_0^\delta\rho U_s\left(\frac{\rho_e}{\rho}-1\right)\left(1-\frac{y}{R}\right)dy-\int_0^\delta\rho U_e\left(\frac{\rho_e}{\rho}-\frac{u}{U_e}\right)\left(1-\frac{y}{R}\right)dy\right\} \tag{5}$$

The integration of this expression from the shock wave ($\xi=0$) to the contact surface ($\xi=1$) gives the following formula:

$$\rho_e(U_s-U_{es})=\frac{2}{R}\left\{\int_0^\delta\rho U_e\left(1-\frac{u}{U_e}\right)\left(1-\frac{y}{R}\right)dy\right\}_c \tag{6}$$

This relation means that the net mass flow through the shock wave is equal to the net mass flow lost through the boundary layer at the contact surface.

Finally, in order to obtain the expression for the limiting separation distance, the variable y must be replaced by η

$$Lm=\frac{1}{W_\ell-1}\frac{D^2}{16}\left(\frac{\rho_e\bar{U}_e}{\mu_e}\right)_s\tilde{\beta}^{-2} \tag{7}$$

where

$$W_\ell=\left(\frac{\rho_{es}}{\rho_1}\right)_\ell;\quad \bar{U}_e=U_s-U_e\quad \tilde{\beta}=\sqrt{2}\int_0^\infty\left(1-\frac{u}{U_{ec}}\right)d\eta$$

This distance Lm is proportional to the cross-section area of the tube and to the limiting Mach number $M_{s\ell}$, and depends on the boundary-layer profile at the contact surface through the quantity $\tilde{\beta}$ when the limiting regime is attained. The

present computation of the unsteady flow enables this regime to be determined with a good approximation and the values for Lm, M_{s_ℓ}, and $\tilde{\beta}$ are directly obtained for the different cases. So it is possible to compare these values (Lm, M_{s_ℓ}) with those coming from steady theories.[4,5]

Equation (7) can be written in two different forms which are more convenient for comparisons with other theories.

$$\frac{Lm}{P_1 D^2} = \frac{1}{16}\frac{M_{s_\ell}}{W_\ell - 1}\left(\frac{\gamma}{a_1}\right)\frac{1}{\mu_{es}}\tilde{\beta}^{-2} = F(M_s, T_1) \qquad (8)$$

and

$$\frac{Lm}{D^2(\rho a/\mu)_1} = \frac{M_{s_\ell}}{W_\ell - 1}\left(\frac{\mu_1}{\mu_{es}}\right)\tilde{\beta}^{-2} \qquad (9)$$

It is possible to deduce the ratio of maximum test time τ_m is ideal shock tube test time τ_{TH} at a given station x_0

$$\left(\frac{\tau_m}{\tau_{TH}}\right)\Big/\left(\frac{P_1 D^2}{x_0}\right) = \frac{M_{s_i}}{M_{s_\ell}}(W_i - 1)F(M_s, T_1) \qquad (10)$$

V. Numerical Results and Comparisons

Numerical results are obtained for a 5-cm-diam shock tube, for initial temperature $T_1 = 295$ K and initial pressure $P_1 = 0.5$ Torr. The value of $P_1.D$ is such that the boundary layer can be considered as laminar.[9] The initial Mach numbers are in the range 3-9. The driver gas is helium and the driven gas is argon. At the initial time $t_0 = 6.10^{-5}$s, the values of the different quantities are calculated by Hugoniot relations in which the shock Mach number has its ideal value. It has been shown that the influence of the initial data line vanishes quickly along the tube.[11,17] On the other hand, the mesh of the plane (ξ,η) was varied from (5×51) to (15×71) nodes. The step time Δt is chosen so as to satisfy the C.F.L. criterion ($\Delta\eta = 0.1$ and $\Delta t = 4\,10^{-6}$s).

A. Separation Distance and Test Time

The driver gas boundary layer chiefly acts on the evolution of the interface which tends to slow down, therefore, the hot flow lengths are larger. This effect increases as the shock Mach number decreases. For the smallest M_s used ($M_{s_i} = 3$) in the present work, the discrepancy for Lm is smaller than 2%, which enables us to neglect the presence of the cold gas boundary layer for the other studied cases ($M_{s_i} = 4,7,9$).

Figure 1a shows, for different initial Mach numbers, the evolution of the separation distance L between the shock and the contact surface along the tube ($x=0$ is diaphragm location). In the shock tube ideal theory, this distance increases linearly. One of the boundary-layer growth effects is that this distance tends to a limiting value Lm. Considering the asymptotic behavior of the phenomenon, the limiting regime is supposed to be reached when the discrepancy between the shock and the interface velocity is 1 m/s. This same figure also shows the asymptotic behavior of Lm as initial Mach number M_{s_i} increases. The relation in Eq. (9) shows that this result could be expected. Figure 1b shows the time evolution of the shock wave and the interface up to the limiting regime.

The present numerical results can be compared easily to Duff's experiments. In a 2.86-diam shock tube with initial pressure $P_1 = 0.5$ Torr and argon as the driven gas, Duff measured the variation of the test time as a function of the shock Mach number at 3.81 m from the diaphragm. At this station, if the limiting regime is reached, it is possible to determine the maximum test time τ_m with the aid of the present computation, and the knowledge that the maximum separation distance Lm is proportional to the square of the radius. The calculated values of maximum test time are in good agreement with Duff's measurements (Fig. 2). In this figure, the analyses of Ackroyd and of Hooker are also represented.

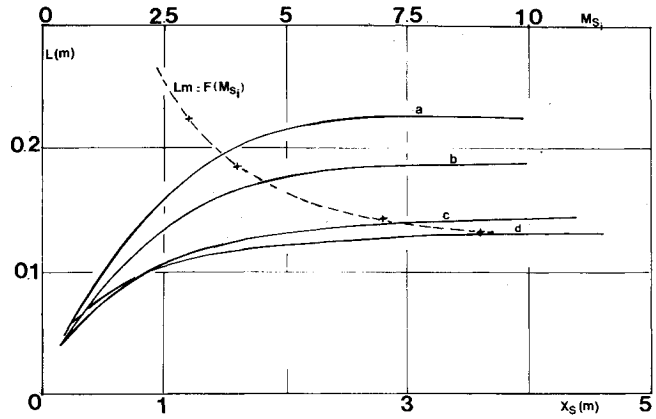

Fig. 1a Evolution of separation distances L along the tube and maximum separation distance Lm against initial shock Mach number M_{s_i}: a) $M_{s_i} = 3$; b) $M_{s_i} = 7$; c) $M_{s_i} = 7$; d) $M_{s_i} = 9$.

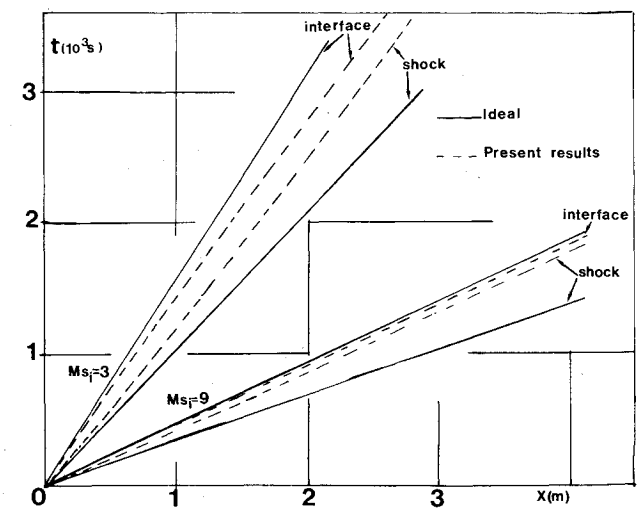

Fig. 1b Evolution of shock wave and interface along the tube up the limiting regime.

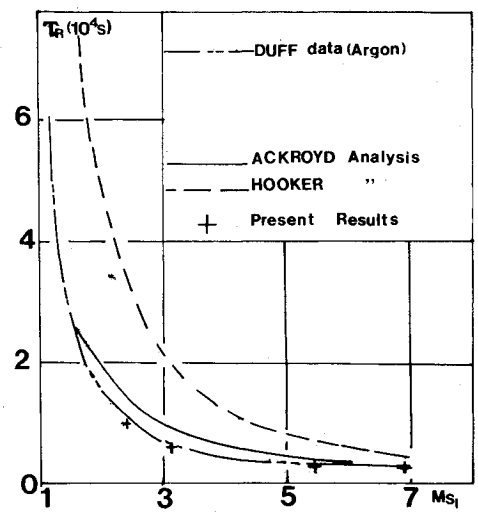

Fig. 2 Comparison of numerical results of test time with Duff data.

B. Shock Wave Attenuation

In the limiting regime, the value of the common velocity of the shock and the interface is independent of the nature and of the rate of growth of the boundary layer; it is a function only

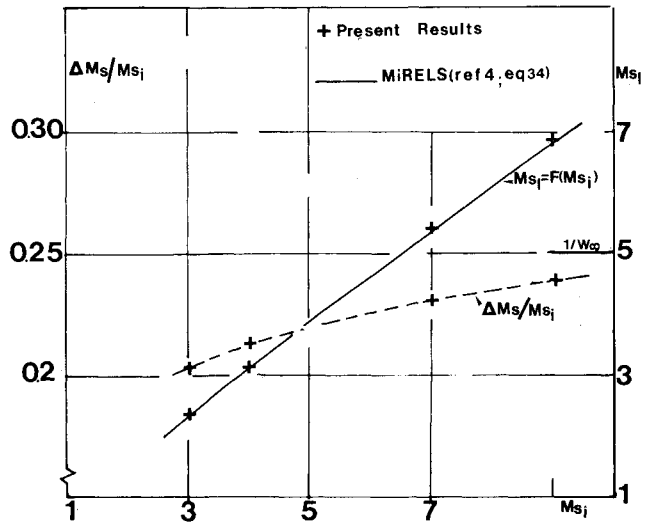

Fig. 3 Comparison of numerical values of limiting Mach number with steady analysis.

of the initial conditions.[1,4] This conclusion has here been verified and it is the same for the previous studies.[11,12] Thus, for $M_{si}=4$ (He/A) the value for M_{sf} is 3.15, for whatever computation method is used for the boundary layer.

Figure 3 represents the relative difference between the initial (M_{si}) and limiting (M_{sf}) Mach numbers. This quantity tends to the value equal to $1/W_\infty=0.25$ when $M_s\to\infty$ in agreement with Roshko's, Mirels', and Musgrove's predictions. The numerical values of M_{sf} are in good agreement with analytic solutions.[4]

C. Comparisons with Mirels' Analysis and Experimental Studies

The numerical determination of the maximum separation distance Lm and the limiting value of Mach number M_{sf} as a limit of the unsteady computation enables us to deduce the values of the parameters $\beta=f(Lm, M_{sf})$ given by Mirels' analysis [Eq. (4), Ref. 4], and to compare with Mirels' expression for the parameter β (noted here as β_M) given by Eq. (17) of Ref. 4, and also with the different values of β (noted here β_{exp}) deduced from experimental data for argon. These results are collected in Table 1. They show the discrepancy between the values of β and β_M. This discrepancy lies between 22% for $M_s\simeq 2.4$ and 14% for $M_S\simeq 7$. This variation is in agreement with Mirels'[4] and Fox's[18] observations and with the experimental data. These different comparisons bring to light the importance of taking into account the spatiotemporal variations of the freestream and the boundary layer to describe the mutual interaction.

The unsteady study of the flow enables us to follow the evolution of the velocity profiles in the boundary layer, and thus it is possible in particular to represent this profile at the contact surface for the limiting regime (or assumed so with a good approximation). Figure 4 shows that the quantity $(1-u/U_{ec})$ across the boundary layer is quasi-independent of the shock Mach number. The parameter $\tilde{\beta}$ deduced by integrating these profiles through the boundary layer is equal to 2.68, within 2% for all computed cases $M_{si}=3,4,7,9$). This result enables us to draw the ratio (Lm/P_1D^2) as a function of Mach number (Fig. 5) and to compare it with Mirels' analysis. Taking account of the unsteadiness of the boundary layer gives boundary-layer thicknesses more important than for the steady studies. Thus, the corresponding values of Lm are smaller.

Table 1 Comparison of β values[a]

	M_{si}/M_{sf}	Lm, m	$\beta=F(Lm, M_{sf})$[b]	$\beta_M=F(M_{sf})$[c]		M_S	β_{exp}
a	3/2.4	0.225	2.54	2.08	Duff	~1.6	3.9
b	4/3.15	0.188	2.22	1.86	Hooker	4	2.2
c	7/5.41	0.143	1.88	1.64	Roshko	5-9	1.8
d	9/6.86	0.132	1.71	1.5	Fox	7-12	1.73

[a] β_{exp} deduced from experimental data; β deduced from numerical values Lm, and M_{sf}; β_M deduced from Mirels' estimate. [b] From Ref. 4, Eq. (4). [c] From Ref. 4, Eq. (17).

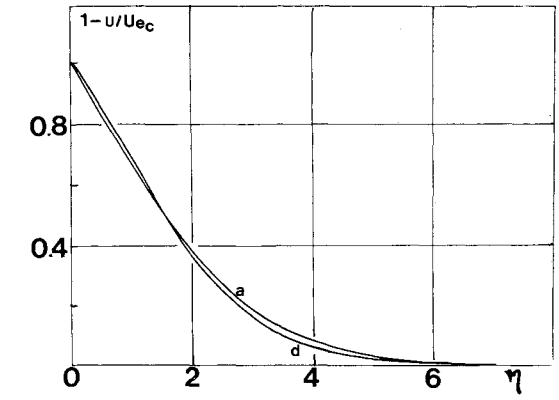

Fig. 4 At limiting regime, velocity profiles across boundary layer at contact surface: a) $M_{si}=3$; d) $M_{si}=9$.

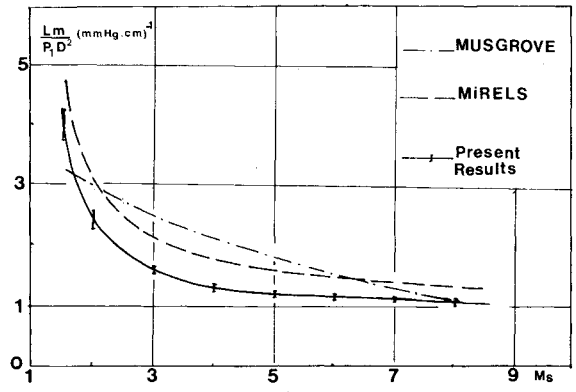

Fig. 5 Maximum separation distance against Mach number for argon.

Using Hooker's experimental conditions ($M_S\simeq 4$, $D=3.95$ cm, $x_0=6.27$ m) and supposing the limiting regime obtained at the station x_0, it is possible to draw τ_m/τ_{TH} as a function of the initial pressure P_1 (relation 10). This evolution is linear and agreement is shown with Hooker's experiments (Fig. 6). This comparison is of course no more valid as $P_1\simeq 4$ Torr (then, the boundary layer is transitional).

D. Flow Variables at the Limiting Regime

At the limiting regime and for the studied Mach number range, Figs. 7-9 represent the variations of the hot flow parameters from shock wave ($\xi=0$) to contact surface ($\xi=1$). As for temperature distributions (Fig. 7), their variation is within 10%,[19] except for the region next to the contact surface where the gradient is much stronger. The origin of this region comes from the choice of the initial data line for which the quantities are assumed constant and also from an interface assumed athermanous.[12] However, in this region the temperature tends to decrease when $t\to\infty$, but very slowly because this decrease comes only from the local mass loss.

The pressure variation (Fig. 8) is more important; it is of the order of 30%-20% depending on the Mach number M_S and as M_S increases the curves tend to superpose. This last conclusion is also true for the velocity distribution (Fig. 9),

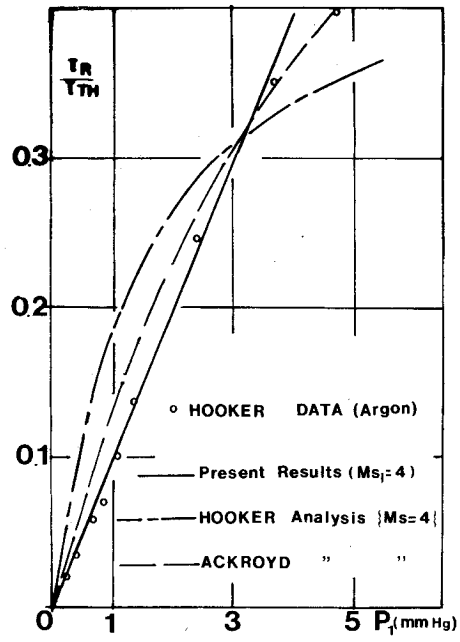

Fig. 6 Comparison of test time at given station against initial pressure for argon.

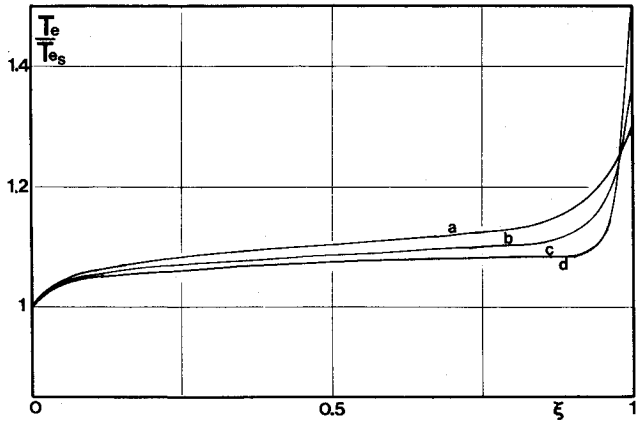

Fig. 7 Temperature profiles in hot flow at the limiting regime: a) $M_{si}=3$; b) $M_{si}=4$; c) $M_{si}=7$; d) $M_{si}=9$.

but the increase is more important for small Mach numbers (60% for $M_S=2.4$).

These different graphs, as a function of the non-dimensional hot flow abscissa ξ, can be compared to the Mirels' analytic expressions.[20] As for temperature and pressure, their distributions are very close and the maximum discrepancy is of the order of 4% for $M_S \simeq 2.4$.

As for velocities, their profiles do not have a parabolic shape as did those found by Mirels for the following hypothesized reason: "the ratio of excess mass flow in a laminar boundary layer at station ξ to the mass flow through the shock varies as $\xi^{1/2}$"; but they have a linear variation with ξ as soon as $\xi > 0.3$. This discrepancy increases when M_S decreases (Fig. 10).

VI. Conclusion

In order to study the hot flow in a low-pressure shock tube, the coupled freestream and boundary-layer equations are numerically solved by taking into account the spatio-temporal variations induced by mutual interaction. Thus, a better knowledge of the unsteady evolution of hot flow is obtained including the distribution of all parameters at the limiting regime and more particularly the values of the maximum separation distance and test time. The present results are in agreement with different experimental results at usual measurement stations.

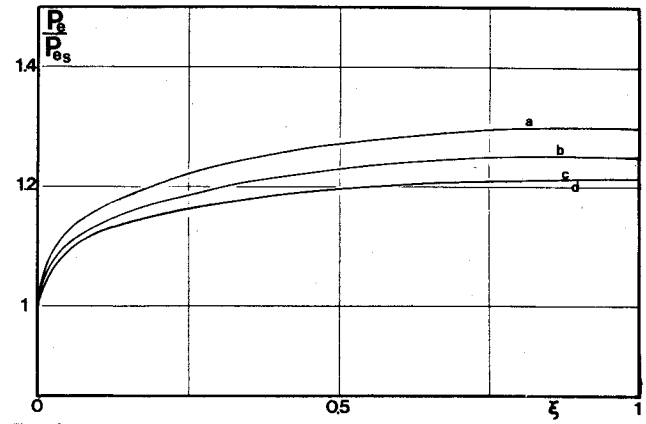

Fig. 8 Pressure profiles in hot flow at the limiting regime: a) $M_{si}=3$; b) $M_{si}=4$; c) $M_{si}=7$; d) $M_{si}=9$.

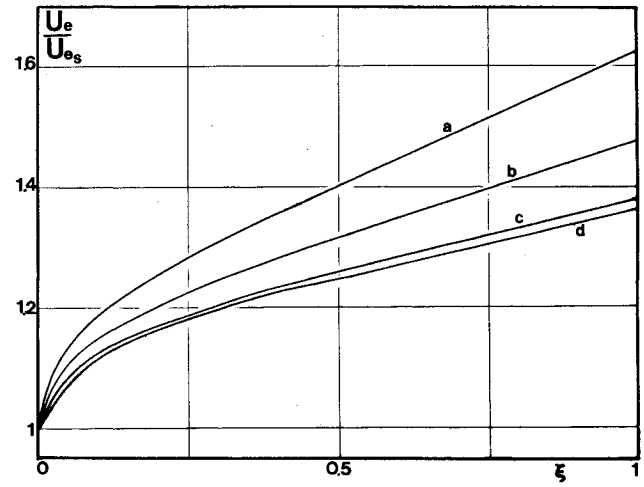

Fig. 9 Velocity profiles in hot flow at the limiting regime: a) $M_{si}=3$; b) $M_{si}=4$; c) $M_{si}=7$; d) $M_{si}=9$.

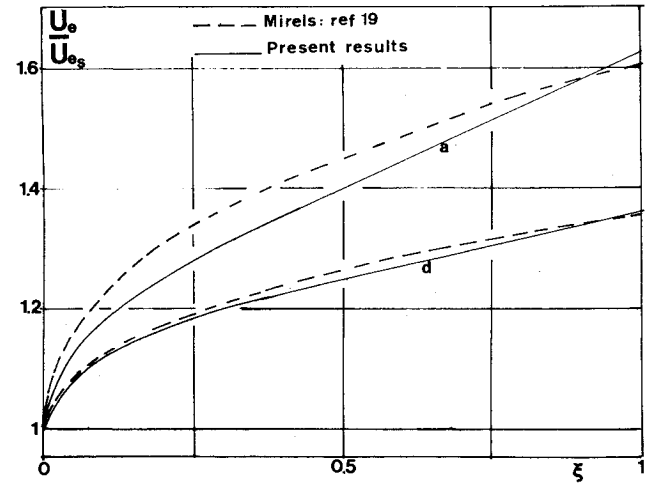

Fig. 10 At the limiting regime, comparison of velocity profiles with Mirels' steady analysis: a) $M_{si}=3$; d) $M_{si}=9$.

Acknowledgments

The authors would like to thank R. Brun for his interest, encouragement, and many helpful comments in the preparation of the manuscript.

References

[1] Duff, R. E., "Shock Tube Performance at Low Initial Pressure," *The Physics of Fluids*, Vol. 2, March-April 1959, p. 207.

[2] Roshko, A., "On Flow Duration in Low Pressure Shock Tube," *The Physics of Fluids*, Vol. 3, Nov. 1960, p. 807.

[3] Hooker, W. J., "Testing Time and Contact Zone Phenomena in Shock Tube Flow," *The Physics of Fluids*, Vol. 4, Dec. 1961, p. 1451.

[4] Mirels, H., "Test Time in Low Pressure Shock Tubes," *The Physics of Fluids*, Vol. 6, Sept. 1963, p. 1201.

[5] Mirels, H. and King, W. S., "Series Solutions for Shock Tube Laminar Boundary Layer and Test Time," *AIAA Journal*, Vol. 4, May 1966, p. 782.

[6] Ackroyd, J.A.D., "A Study on the Running Times in Shock Tubes," Aeronautical Research Council 24942, 1964.

[7] Bernstein, L., "Notes on Some Experimental and Theoretical Results for the Boundary Layer Development Aft the Shock in a Shock Tube," Aeronautical Research Council, CP 625, 1963.

[8] Musgrove, P. J. and Appleton, J. D., "The Influence of Boundary Layer Growth on Shock Tube Test Time," *Applied Scientific Research*, Vol. 18, Sept. 1967, p. 116.

[9] Mirels, H., "Boundary Layer Growth Effects in Shock Tube," *Proceedings of 8th International Shock Tube Symposium*, Imperial College, London, June 1971.

[10] Spence, D. A. and Wood, B. A., "A Review of Theoretical Treatment of Shock Tube Attenuation," *Journal of Fluid Mechanics*, Vol. 19, June 1964, p. 161

[11] Sides, J. and Brun, R., "Méthode Numérique de Détermination des Grandeurs de l'Ecoulement dans un Tube a Choc Compte Tenu de la Couche Limite Pariétale," *Journal of Mécanique*, Vol. 14, No. 3, 1975, p. 387.

[12] Brun, R. and Imbert, M., "On an Improved Calculation Method of Shock Tube Flow," *Proceedings of 10th International Shock-Tube Symposium*, edited by G. Kaminoto, Kyoto, Japan, 1975.

[13] Dem'Yanov, Y. A., "The Influence of the Boundary Layer on the Character of the Flow of the Gas in a Tube Behind a Moving Shock Wave," *Prikladnaia Mathematika i Mekhanika*, Vol. 21, 1957, p. 473.

[14] Hartree, D. R., *Numerical Analysis*, Oxford University Press, 1958, Chap. X.

[15] Tong, K. O. and Russel, D. A., "Viscous Effects in Tube Flow Initiated by an Expansion Wave," *AIAA Journal*, Vol. 15, Dec. 1977, p. 1763.

[16] Blottner, F. G., "Investigation of Some Finite Difference Techniques for Solving the Boundary Layer Equations," *Computer Methods Appl. Mech. Engineering Neterlands*, Vol. 6, Jan. 1975.

[17] Zeitoun, D. and Imbert, M., "Méthode Numériqu̧e de Détermination de la Couche Limite Instationnaire Associé a un Ecoulement Extérieur non Uniforme: Applicaton au Tube a Choc," *Journal de Mécanique*, Vol. 16, No. 1, 1977, p. 1.

[18] Fox, J. N., McLaren, T. I., and Hobson, R. M., "Test Time and Particle Paths in Low Pressure Shock Tube," *The Physics of Fluids*, Vol. 9, Dec. 1966, p. 2345.

[19] Holbeche, T. A., "A Theoretical and Experimental Investigation of Temperature Behind Attenuating Shock Waves," *Proceedings of the Royal Society*, Vol. A279, 1963, p. 111.

[20] Mirels, H., "Flow Non Uniformity in Shock Tubes Operating at Maximum Test Time," *The Physics of Fluids*, Vol. 9, Oct. 1966, p. 10.